Available online at www.sciencedirect.com
SCIENCE DIRECT®
International Journal of Heat and Mass Transfer 49 (2006) 259–268
International Journal of HEAT and MASS TRANSFER
www.elsevier.com/locate/ijhmt

Studies on critical heat flux in flow boiling at near critical pressures

B.R. Vijayarangan, S. Jayanti, A.R. Balakrishnan *

Department of Chemical Engineering, Indian Institute of Technology Madras, Chennai 600 036, India

Received 20 January 2005; received in revised form 27 May 2005
Available online 21 September 2005

Abstract

Experimental studies on critical heat flux (CHF) have been conducted in a uniformly heated vertical tube of 12.7 mm internal diameter and 3 m length at different reduced pressures ranging from 0.24 to 0.99 with R-134a as the working fluid. The onset of CHF was determined by the sudden rise in the wall temperature of the electrically heated tube. Experiments were performed over a wide range of parameters: mass flux values from 200 to 2000 kg/m^2 s, pressure from 10 to 39.7 bars and heat flux from 2 to 80 kW/m^2 and exit quality from 0.17 to 0.94. The results show considerably lower critical heat flux at high pressures. Well known CHF prediction methods, such as the look-up table and correlations of earlier workers show poor agreement at high pressures. A new correlation has been proposed to estimate the CHF in uniformly heated vertical tubes up to the critical pressure and over a wide range of parameters.

1. Introduction

Critical heat flux (CHF) in flow boiling is that heat flux that results in a sudden rise in the wall temperature. There are basically two classes of CHF situations, namely departure from nucleate boiling (DNB) and dryout (DO). DNB occurs at very low qualities or even under sub-cooled liquid conditions; here the vapour generation rate is higher than the rate of vapour evacuation by the flowing liquid. This leads to an accumulation of vapour at the generation site and prevents liquid from contacting the surface. The vapour therefore gets superheated and the wall temperature rises suddenly due to the relatively poor heat transfer characteristics of vapour. In contrast to DNB, dryout occurs at high qualities and is a result of the gradual disappearance of the liquid film adjacent to the wall as a result of both entrainment and evaporation. Dryout occurs in annular flow and a significant amount of liquid may still be flowing in the form of droplets entrained by the vapour [1]. Dryout which occurs at much lower heat fluxes than DNB, has been recognized as a limiting condition in flow boiling and is the subject of the present study.

Critical heat flux has been studied extensively over the past several decades. Authoritative reviews on the subject have been given from time to time (reviews each from [2–4]), and a number of mechanisms for the occurrence of DNB and DO have been identified. Four principal approaches to prediction of CHF have evolved over the years. These are: the empirical correlation approach used since the early 60s; the dimensional approach pioneered by Katto and Ohno [5], the phenomenological approach initiated in the 1970s [6] and fined tuned in the 1990s [7]; and the look-up table

* Corresponding author. Tel.: +91 44 2257 8209; fax: +91 44 2257 0509.
E-mail address: arbala@iitm.ac.in (A.R. Balakrishnan).

0017-9310/$ - see front matter © 2005 Elsevier Ltd. All rights reserved.
doi:10.1016/j.ijheatmasstransfer.2005.06.029

Nomenclature

D	diameter, m
G	mass flux, kg/m^2 s
g	acceleration due to gravity, m/s^2
K	inlet subcooling parameter
L	length of the tube, m
P	absolute pressure, bar
Pr	Prandtl number, $\mu c_p/k$
P_R	reduced pressure P/P_{cr}
q	critical heat flux, kW/m^2
Re	Reynolds number, Gd/μ
X	function of dimensionless parameters
x	mass fraction or quality
z	the distance at which the wall temperature rose

Greek symbols

ΔHs	inlet subcooling enthalpy, kJ/kg
ΔT_{sub}	inlet subcooling, °C
μ	viscosity, Ns/m^2
λ	latent heat of evaporation, kJ/kg
ρ	density of gas, kg/m^3
σ	surface tension, N/m

Subscripts

cr	critical
CHF	critical heat flux
imp	imposed
l	liquid
R	reduced (pressure)
v	vapour

Superscripts

$m = 0.147$
$n = 0.25$

method, initiated by the USSR Academy of Sciences [8] and later adopted and extended by Groeneveld and co-workers [9–12]. Together, these have provided a basis for the prediction of CHF over the years. Of these several approaches, the purely empirical one of the early 60s has been abandoned and the other three are still used. The CHF look-up table method is a purely statistical (numerical) technique and does not include any physics of the situation in its prediction; however, it is the most accurate approach if sufficient data is available. The phenomenological approach is the most reliable as it is a mechanistic model; however, it does require a lot of empirical input in the form of rates of entrainment and redeposition, etc. The generalized CHF correlation approach depends on dimensional analysis, and although it presents a relatively simple way of predicting CHF, it depends strongly on empirical data to determine the constants appearing in the dimensionless correlations.

Most of the available work on CHF has been done for water as the working fluid and have been confined to relatively low pressures. Thus, the phenomenological modeling approach has been verified up to a reduced pressure (P/P_{cr}) of 0.3, that is, up to a pressure of 70 bar for a steam-water system [7]. Recent attempts have been made [13,14] to extend it to higher pressures. However, it was found that the original hydrodynamic entrainment–redeposition model, which had worked well up to the reduced pressure of 0.3, was inadequate in itself to predict dryout at much higher pressures and that other factors such as nucleation-induced entrainment and vapour-inhibited redeposition became important. Thus, straightforward extension of low pressure correlations and models may not be satisfactory at high pressures. Yet another problem with the existing body of work is that most of the available data is for conventional fluids, namely, water and freons. Although considerable amount of data of convective boiling heat transfer exists on new refrigerants (see review by Thome [15]), most of it is confined to low pressures, typically, for a reduced pressures of less than 0.25. Not much data on CHF is available for R-134a and other new refrigerants. Pioro et al. [16] measured CHF for R-134a for vertically upward flow in the pressure range of 0.96–2.39 MPa (reduced pressure range of 0.25–0.60) for mass fluxes in the range of 500–3000 kg/m^2 s over a range of inlet qualities. They found good agreement with the look-up table method of Groeneveld [12]. However the agreement became progressively worse as the system pressure increased.

The objective of the present study is therefore to obtain critical heat flux data for R-134a over a range of pressures approaching critical pressure. This would fill the void in CHF data at near-critical pressures, in general and on R-134a in particular. Using fluid-to-fluid scaling laws, these data can then be extended to other fluids as well. With this in view, CHF experiments were conducted in vertical up-flow over a range of system pressures, mass flux and heat flux with a fixed inlet subcooling.

2. Experimental

The schematic diagram of the experimental set-up, is designed and fabricated for the present study is shown in

Fig. 1. The test rig consists of the primary loop (working fluid), the chilling unit loop, the cooling water loop and the data acquisition system. These are described below.

In the primary loop the working fluid, R-134a, flows in a closed circuit. It consists of a refrigerant pump, an accumulator, a mass flow meter, the test section, a filter, pressure transducers, a pressure regulating valve and a receiver tank. The refrigerant is circulated through the loop by a hermetically sealed oil-free canned motor pump. A piston type accumulator is used to vary and maintain the desired pressure level of the loop. A calibrated micromotion mass flow meter (Fisher Rosemount of type R-series) is used to measure the mass flow rate at the delivery of the pump. A flow and pressure regulating valve is positioned in between the mass flow meter and the pump. The required flow rate at the test section can be set by operating the main and bypass valves provided at the pump delivery. The vertical upflow test section is positioned after the mass flow meter as shown in Fig. 1. The liquid–vapour mixture from the test section passes through the cooling loop and the condensed liquid is fed to the receiver tank connected to the suction end of the pump.

The chilling unit loop is another closed loop system which enables the test fluid, R-134a, in the primary loop to be operated at pressures as low as 1 bar and as high as the critical pressure (40.56 bar). It contains three condensers connected in parallel and designed to work at different pressures and temperatures. The first condenser works in the temperature range of +30 to +100 °C corresponding to a test section pressure in the (range 7–40.56 bar) and uses tap water as the heat sink. The condenser works with cooling water on the shell side and the refrigerant R-134a on the tube side. The cooling water is circulated through a 3 HP pump. The required flow rate of the cooling water can be set by adjusting the main valve and the bypass valve. The flow rate is measured by a rotameter positioned on the delivery side of the pump. The inlet and outlet temperatures of the cooling water are measured using T-type thermocouples. The second and the third condensers are designed to operate in the temperature ranges of 0 to 30 °C and −30 to 0 °C, respectively, which corresponds to test section pressures of 3–7 bar and 1–3 bar, respectively. These two condensers form a closed loop with a refrigerant mixture of R-12 and R-404a providing the heat sink to the primary coolant. The chilling unit loop is equipped with an hermetically sealed compressor to circulate the refrigerant mixture through the condenser units. The condensers are shell-and-tube heat exchangers in which R-134a flows on the tube side and R-12 and R-404a mixture on the shell side. Depending on the operating pressure and temperature of the test fluid in the primary loop, only one of the condensers is operated at any time.

The test set-up was subject to a hydrostatic pressure test at up to 60 bar to ensure leak free operation at 40 bar with R-134a. Before filling up the test loop with R-134a, a vacuum of the order of 0.1 Pa was created using a vacuum pump to ensure no other gases other than the refrigerant is present.

The test section is made of stainless steel (SS-304) and has an inner diameter of 12.7 mm and an outside diameter of 16.7 mm. The heated length of the test section is 3 m. A low voltage, high current DC power supply (maximum of 17 V DC, 800 A) is used to heat the test

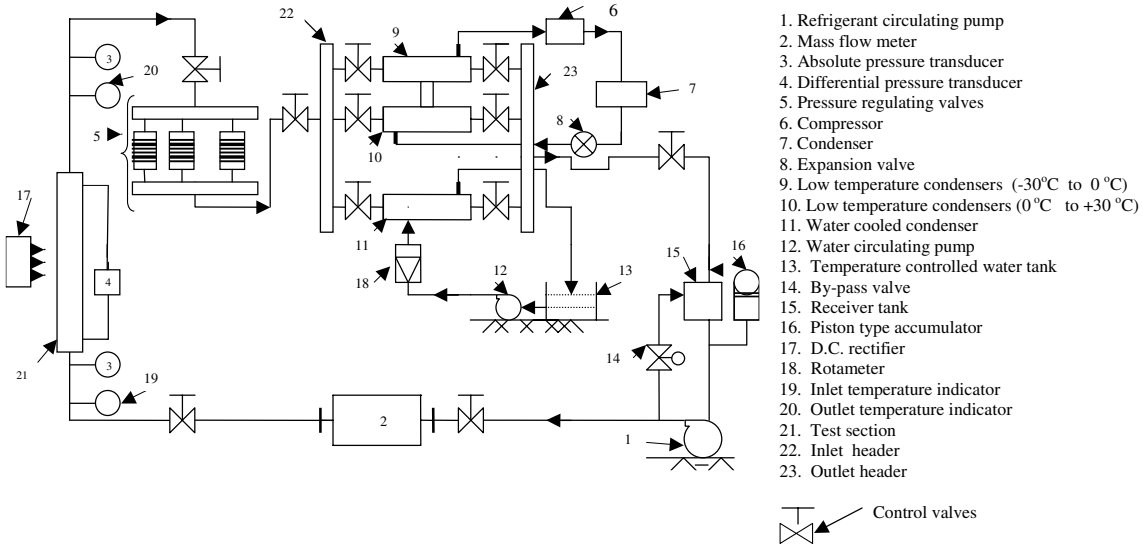

Fig. 1. Schematic diagram of test loop.

section. The DC power is supplied through two copper bus bars of 100 mm width and 7 mm thickness connected across the test section of 3 m. The test section is well-insulated with asbestos rope and polyurethylene foam to minimize heat losses to the surroundings.

Details of the instrumentation on the test section are shown in Fig. 2. The bulk fluid temperature is measured at the inlet (T_{fi}), at the outlet (T_{fo}) of the test section and at four other intermediate locations using mineral insulated T-type thermocouples of 1.10 mm bead diameter. The wall temperature of the test section is measured at 40 axial locations along the heated length using T-type thermocouples of bead diameter 0.8 mm. All the thermocouples are isolated from any disturbance signals from the DC power supply by a Galvanic signal isolator. The thermocouples were calibrated before installation as well as in-situ. The nominal accuracy of each thermocouple is 0.1 °C.

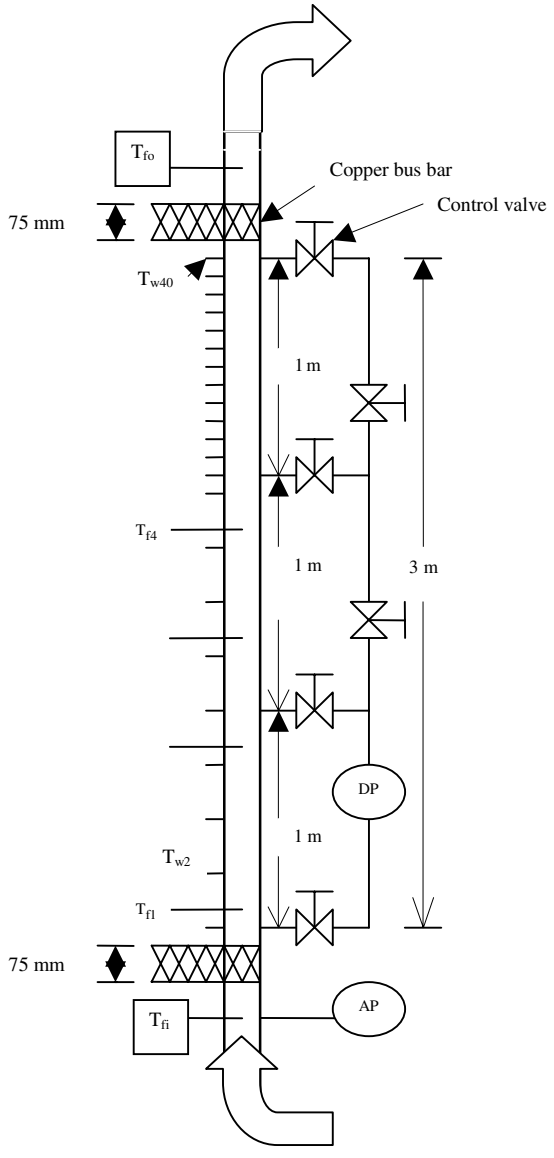

Fig. 2. Test section details.

A differential pressure transducer is used to measure the pressure drop across the test section. In addition, absolute pressure transducers are located at the test section inlet and outlet. These pressure transducers are calibrated with an uncertainty of ±0.5% of the full-scale value. The pressure transducers are electrically isolated by providing teflon seating and bushes in-between the flanges and bolts to which the transducers are connected.

A Contec-make ADI12 PC and an ATP M3 type analog-to-digital add-on cards are used to process ±5 V DC signals from the measuring instruments and all the millivolt (mV) signals from the thermocouples, respectively. A data acquisition code which includes all calibration equations and conversions to desired engineering units, is used to provide on-screen display of analog signals from the sensors. The sensor output voltages are time-averaged for the mean quantities of pressure, temperature and flow rates. As a check on steady state, three data sets are compared for consistency before all the scans are averaged together for further processing. The end result is a set of measurements, each an average of 10 readings, and a confirmation of steady state system operation during the collection of data. Signals from all the sensors are processed through a data acquisition system consisting of a PC and a multiplexer and the output is stored on the hard disk of the computer.

In a typical experiment, R-134a from the storage tank is circulated through the test section, condensed and then recirculated using the hermetically sealed pump. For a set value of pressure, flow rate, inlet subcooling and heat flux, the rise in the tube wall temperature is monitored. If a sudden rise in the wall temperature at any location is not detectable, then heat flux (power input) is increased and the wall temperature is again observed. This process is continued until one of the thermocouples shows a significant rise in wall temperature. The power supply is shut-off automatically when one of the measured wall temperatures exceeds a given limiting value (150 °C in the present study). These experiments are repeated for different flow conditions. The pressure in the test loop is adjusted by turning on the piston accumulator. The temperature of the fluid at the inlet to the test section is maintained by controlling the temperature and the flow rate of cooling water through the heat exchangers. The flow rate is adjusted using control valves.

The experiments were conducted in the pressure range of 10–39.7 bar in the test section (reduced pressures in the range of 0.24–0.99) and with a mass flux in the range of 200–1000 kg/m^2 s. The inlet subcooling

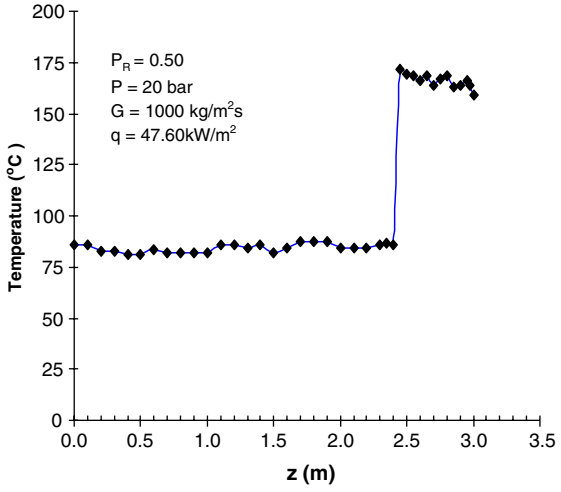

Fig. 3. Location of sudden rise in wall temperature.

was maintained at 3 °C for all cases. Experiments were also conducted at higher mass fluxes range of 1000–2000 kg/m^2 s where the wall temperature was measured at fixed heat fluxes of 35, 60 and 80 kW/m^2 while varying the mass flux for a fixed test section pressure and inlet subcooling. The wall temperature showed a sudden rise after a certain distance from the inlet, as shown in Fig. 3. The CHF here corresponds to the dryout condition. If z is the distance at which the wall temperature rose suddenly and L is the total heated length, the critical heat flux (assuming that for a given set of pressure, mass flux and inlet subcooling, the dryout occurred at the same quality) is given as

$$q_{\mathrm{CHF}} = q_{\mathrm{imp}} \times \left(\frac{z}{L}\right) \tag{1}$$

where q_{imp} is the imposed heat flux.

3. Results and discussion

Critical heat flux experiments were carried out over a range of test section pressures and mass fluxes with a fixed inlet subcooling of 3 °C. The range of parameters investigated in the present study is summarized in Table 1.

The principal parameters investigated in the present study were the system pressure and the mass flux. The inlet subcooling was kept constant at 3 °C for all the experiments. For CHF resulting from high quality dryout, the inlet enthalpy is not expected to be an important factor in determining the quality at which dryout would occur. The experimental data of Bennett et al. [17] and Becker et al. [18] for steam-water systems, as well as the current data show that for a fixed system pressure and inlet mass flux, the quality at which dryout occurs is largely unaffected by the heat flux. The location of dryout would however change along the length of the test section.

Table 1
Range of parameters investigated in the present study

P (bar)	10, 15, 20, 25, 30, 32, 34, 36, 38, 39.7
P/P_{cri}	0.24, 0.37, 0.49, 0.62, 0.75, 0.80, 0.85, 0.90, 0.95, 0.99
G (kg/m^2 s)	200, 400, 600, 800, 1000, 1200, 1400, 1600, 1800, 2000
q (kW/m^2)	35, 60, 80 and variable in the range of 2.8–80
ΔT_{sub}	3 °C

Fig. 4 shows the dependence of CHF on system pressure and inlet mass flux. The measured CHF is plotted against the reduced pressure at mass fluxes of 200, 600, 1200 and 2000 kg/m^2 s. Fig. 4c and d contain CHF data obtained with a fixed wall heat flux (of 35, 60 or 80 kW/m^2) and varying mass flux in which the CHF value was obtained using Eq. (1) above. The fact that there is good agreement for CHF for different imposed heat flux values shows that the DO quality is largely unaffected by the heat flux and that the application of Eq. (1) is justified. Fig. 4 shows that for a given mass flux, CHF decreases, as expected, as the system pressure increases. In general, the CHF is less for low mass fluxes and a significant effect of mass flux is seen at high pressures (reduced pressure >0.75). This effect is clearly seen in Fig. 5 where the CHF at mass fluxes of 400, 800 and 1400 kg/m^2 s are compared at different pressures. The CHF data obtained in the present study is given in Appendix A.

Two well-established methods of predicting CHF, namely, the look-up table method of Groeneveld et al. [9] and the generalized CHF correlation of Katto and Ohno [5] have been used for the comparison with the present data. Fig. 6 shows the comparison between the data and the predictions for mass fluxes of 400 and 1800 kg/m^2 s. Fair agreement with the data is found for low reduced pressures ($P_{\mathrm{R}} < 0.5$), however significant deviation is found from both methods at higher reduced pressures. The CHF predicted by the correlation of Katto and Ohno [5] shows, in addition, a discontinuous behavior. This is because they proposed different CHF correlations in different ranges of parameters (K and X in their correlation). The range of parameters (pressure, mass flux and fluid properties) studied in the present work is such that different CHF correlations are needed for different parameter values. The fact that the experimental data do not show a distinctly different behaviour means that the transition criteria proposed by Katto and Ohno [5] (which are based on low pressure data) cannot be extended to high reduced pressures.

The overall comparison for the two prediction methods for the data points from the present study is shown in Figs. 7 and 8. It is clear from these figures that both prediction methods suffer from large over prediction at high reduced pressures. While part of this

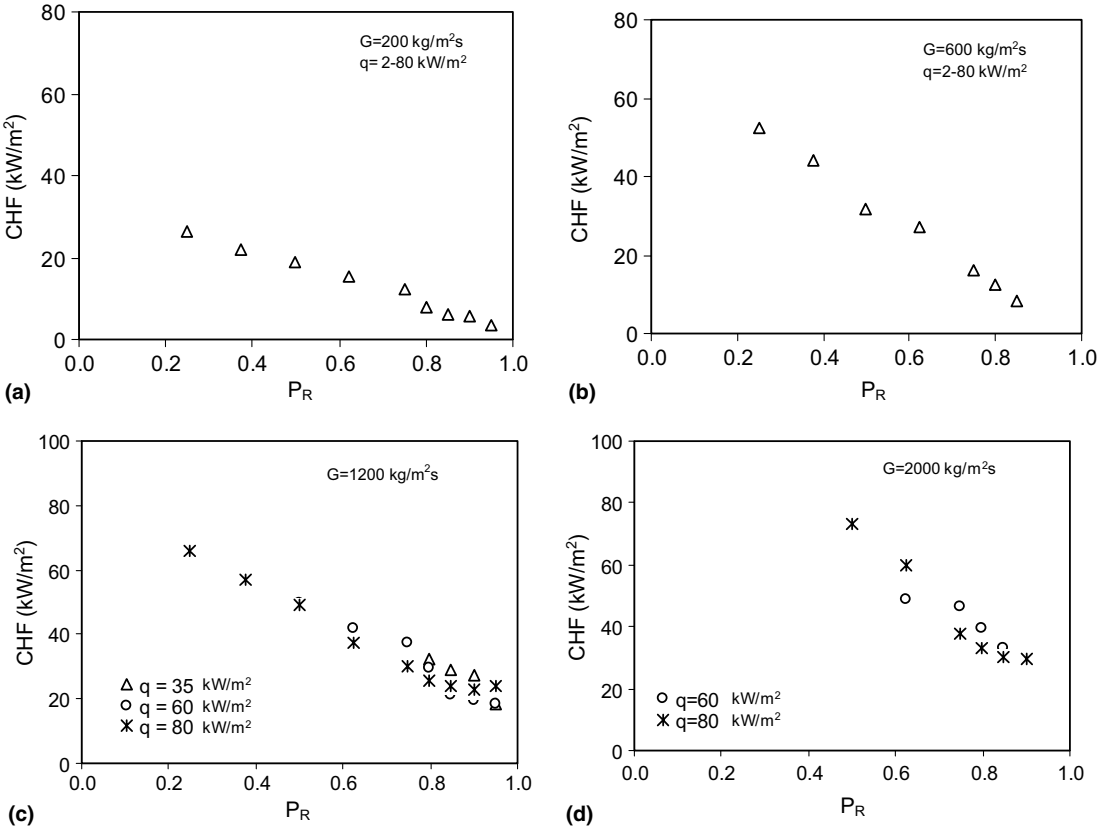

Fig. 4. Measured CHF against reduced pressure for different mass flux values.

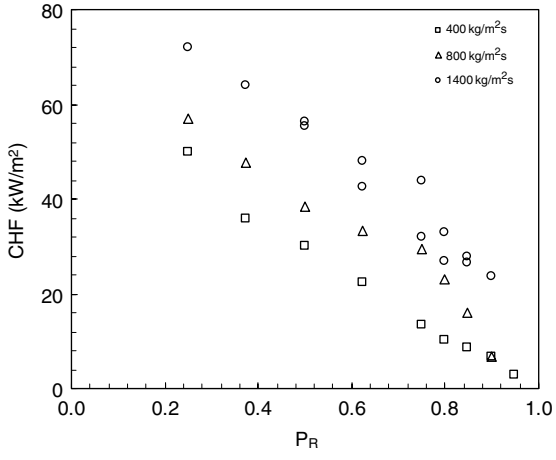

Fig. 5. Influence of mass flux on measured CHF at different reduced pressures.

overestimation is certainly due to the low value of CHF at high reduced pressures (which tends to inflate the relative error), there appears to be a case for correction at high pressures.

Experiments have shown that the critical heat flux is a function of a number of parameters even for a uniformly heated vertical tube. The principal variables that have been identified are the system pressure, thermophysical properties of the fluid, and geometric dimensions of the tube such as the inner diameter and length, mass flux, heat flux and DO quality. A number of attempts have been made to derive dimensionless groups relevant to the critical heat flux [19,20,5,21].

Katto and Ohno [5] analyzed a large body of data collected from a number of sources and correlated them as

$$\frac{q_{\mathrm{CHF}}}{G\lambda} = X + XK\frac{\Delta Hs}{\lambda} \tag{2}$$

where X, $K = f(L/d, \rho_l/\rho_v, \rho_l/G^2L)$.

They proposed a suite of four correlations to capture the functional dependence of CHF on the parameters X and K over a range of flow conditions. However, as shown in Fig. 6 earlier, the predictions of these correlations are not satisfactory, especially at high pressure.

An examination of the four correlations of Katto and Ohno [5] with the present data showed that their second correlation,

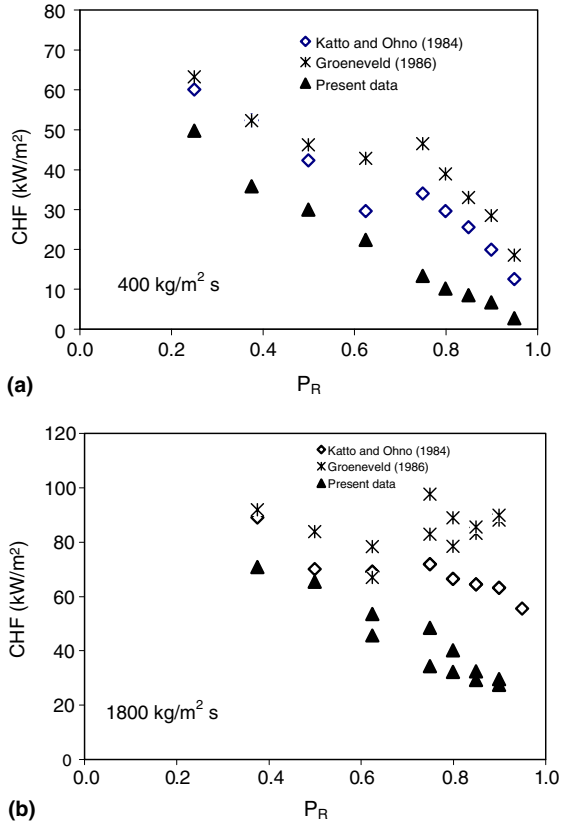

Fig. 6. Comparison of present CHF data with predictions from existing methods.

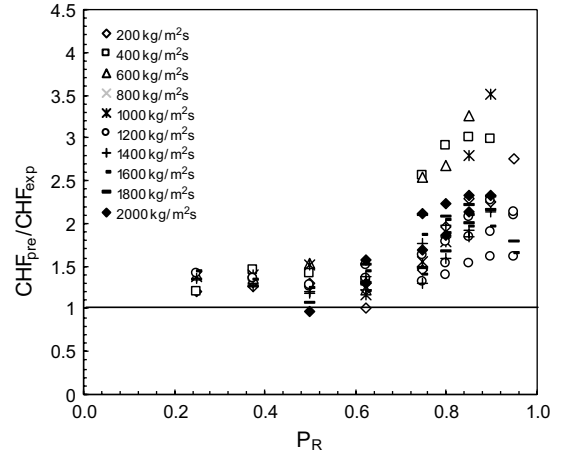

Fig. 7. Comparison of Katto and Ohno [5] correlation with present data.

$$q_{\mathrm{CHF}}/G\lambda = C_1 \times \left\{ (\rho_v/\rho_l)^{0.133} (\sigma\rho_l/G^2L)^{1/3} \times \left(\frac{1}{1+0.0031(L/d)} \right) \right\} \quad (3)$$

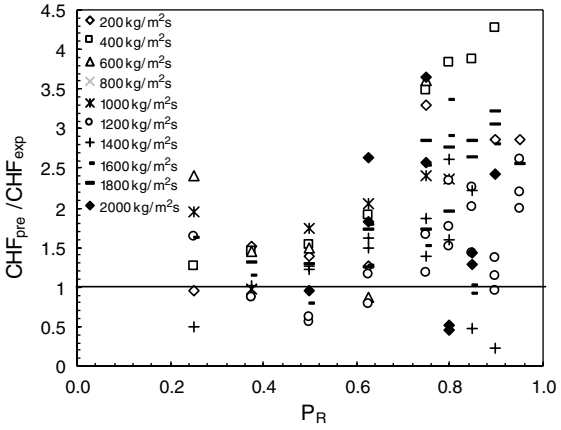

Fig. 8. Comparison of Groeneveld [9] predictions with present data.

came closest to representing the current data. Keeping in mind the strong mass flux effect on CHF as illustrated by Fig. 5 and the significant overprediction of CHF at near-critical pressures (Fig. 6), the above correlation has been modified by including two additional groups, namely, Re_l representing the mass flux and P_R representing the pressure effect. Accordingly, a revised CHF correlation is proposed. The constants were obtained using regression with the present data.

$$q_{\mathrm{CHF}}/G\lambda = 0.0051 \times \left\{ (\rho_v/\rho_l)^{0.133} (\sigma\rho_l/G^2L)^{1/3} \times \left(\frac{1}{1+0.0031(L/d)} \right) P_R^{0.147} Re_l^{0.25} \right\} \quad (4)$$

The performance of this correlation against the current data is compared in Fig. 9 in the form of relative error with pressure. It is seen that fairly good prediction of the CHF is obtained over the range of system pressures and that the large pressure bias seen in the predictions of Groeneveld et al. [9] and of Katto and Ohno [5] has been considerably reduced.

The range of parameters groups over which the above correlation has been obtained is as follows:

$$1.40 \times 10^4 < Re_l < 7.6 \times 10^5$$
$$1.0 \times 10^{-8} < We_l < 1.5 \times 10^{-5}$$
$$6.1 \times 10^{-5} < q_{\mathrm{CHF}}/G\lambda < 8.05 \times 10^{-4}$$
$$0.13 < P_R < 0.95$$
$$0.01 < \rho_v/\rho_l < 0.44$$

The correlation obtained above for R-134a data has been compared with the steam-water data of Becker et al. [18] obtained in a uniformly heated tube of 14.9 mm internal diameter and 7 m length. This is shown in Fig. 10. The experiments were conducted in the pressure range of 30–200 bar (covering a reduced pressure range of 0.13–0.90) and with the mass flux ranging from

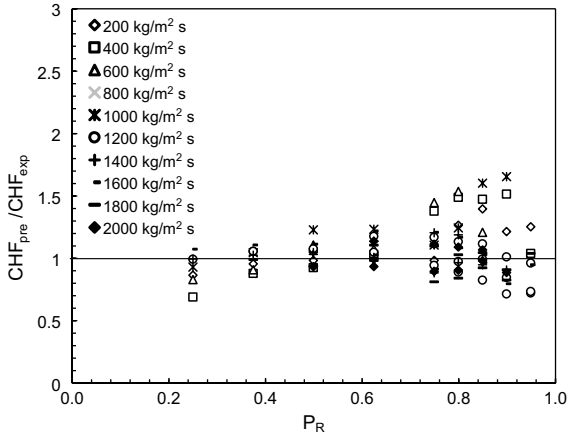

Fig. 9. Performance of the proposed correlation.

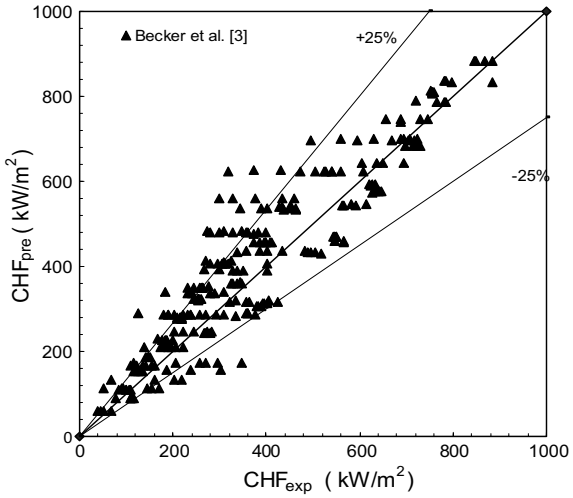

Fig. 10. Performance of the proposed correlation (parity plot) with experimental data of Becker et al. [18].

500 to 3000 kg/m^2 s at a nearly constant inlet subcooling of 10 °C. A constant heat flux was imposed and the wall temperature was recorded; thus, no effort was made in the experiments to obtain DO at the end of the 7-m long test section. In view of this, the imposed heat flux was adjusted using Eq. (1) above to arrive at the experimental value of the CHF. It was noted that in some cases, CHF occurred at very low qualities, sometimes even for subcooled conditions. Only those data points for which the DO quality was higher than 0.1 were taken here for comparison. This yielded 277 points covering a wide pressure and mass flux range. Fig. 10 shows that the proposed correlation predicts these 277 data very well with an average deviation of only 5%. Most of the data lie within the ±15% range; most of the data lying outside this range correspond to data obtained at

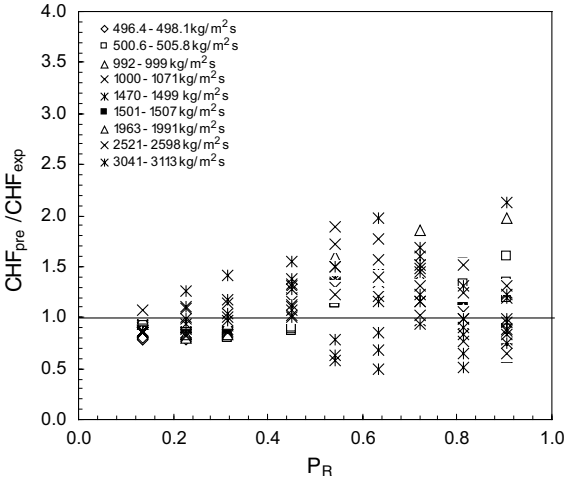

Fig. 11. Performance of the proposed correlation with experimental data of Becker et al. [18] as a function of reduced pressure.

$Re_l > 300{,}000$. The relative error is plotted against reduced pressure and is shown in Fig. 11 and it may be seen that there is no significant pressure bias in the proposed correlation. Thus, the correlation is applicable to both R-134a and steam-water systems over the reduced pressure range of 0.13–0.95.

In the present study the measured variables are the liquid temperature, wall temperature, absolute pressure, mass flow rate, volt and current. The uncertainty in the measurement of temperature is ±0.1%. The uncertainty in the measurement of mass flow rate is ±0.5%. The uncertainty in the measurement of pressure is ±0.25%. The uncertainty in the measurement of volt and current is ±1% and ±1% respectively. Therefore uncertainty in the measurement of critical heat flux lies within 4.46%.

4. Conclusion

Systematic experiments of CHF have been conducted over a range of system pressures and mass fluxes for a uniformly heated tube with R-134a as the working fluid. The critical heat flux decreases monotonically and steadily over the entire range of pressures right up to the critical pressure. Existing prediction methods such as the look-up table method of Groeneveld et al. [9] and the generalized correlation approach of Katto and Ohno [5] have been found to overpredict by a large margin of the CHF data at high system pressures. The correlation of Katto and Ohno [5] has been modified (Eq. (4)) by adding two dimensionless groups. This modification eliminates the pressure bias seen in the earlier correlations of Katto and Ohno [5] and fits both R-134a and steam water data.

Acknowledgement

The second and third author wish to thank the IITM-ISRO cell for sponsoring the above project.

Appendix A

Present experimental data on CHF

Serial no.	P (bar)	P_R	G (kg/m^2 s)	Dryout quality	Heat flux (kW/m^2)
1	10	0.25	200	0.97	26.4
2	15	0.37	200	0.93	22.0
3	20	0.50	200	0.89	18.8
4	25	0.62	200	0.81	15.4
5	30	0.75	200	0.71	12.4
6	32	0.80	200	0.49	7.9
7	34	0.85	200	0.47	6.0
8	36	0.90	200	0.45	5.5
9	38	0.95	200	0.39	3.6
10	10	0.25	400	0.91	49.8
11	15	0.37	400	0.75	35.9
12	20	0.50	400	0.71	30.0
13	25	0.62	400	0.57	22.4
14	30	0.75	400	0.33	13.3
15	32	0.80	400	0.27	10.2
16	34	0.85	400	0.33	8.5
17	36	0.90	400	0.24	6.7
18	38	0.95	400	0.12	2.8
19	10	0.25	600	0.63	52.4
20	15	0.37	600	0.61	44.0
21	20	0.50	600	0.49	31.8
22	25	0.62	600	0.45	27.2
23	30	0.75	600	0.25	16.1
24	32	0.80	600	0.21	12.5
25	34	0.85	600	0.20	8.2
26	10	0.25	800	0.51	57.1
27	15	0.37	800	0.49	47.8
28	20	0.50	800	0.44	38.5
29	25	0.62	800	0.41	33.4
30	30	0.75	800	0.38	29.6
31	32	0.80	800	0.32	23.0
32	34	0.85	800	0.31	16.1
33	36	0.90	800	0.22	6.6
34	10	0.25	1000	0.45	63.2
35	15	0.37	1000	0.42	51.6
36	20	0.50	1000	0.35	38.6
37	25	0.62	1000	0.30	32.0
38	30	0.75	1000	0.27	28.6
39	32	0.80	1000	0.21	20.9
40	34	0.85	1000	0.20	13.4
41	36	0.90	1000	0.12	10.6
42	32	0.80	1200	0.341	32.6
43	34	0.85	1200	0.330	29.1
44	36	0.90	1200	0.313	27.4
45	38	0.95	1200	0.201	18.5
46	15	0.37	1200	0.38	56.8
47	20	0.50	1200	0.37	49.9
48	25	0.62	1200	0.35	42.0
49	30	0.75	1200	0.33	37.5
50	32	0.80	1200	0.31	29.8
51	34	0.85	1200	0.23	21.5
52	36	0.90	1200	0.19	19.4
53	38	0.95	1200	0.20	18.2
54	10	0.25	1200	0.40	65.8
55	15	0.37	1200	0.38	56.8
56	20	0.50	1200	0.36	49.1
57	25	0.62	1200	0.28	37.4
58	30	0.75	1200	0.27	30.2
59	32	0.80	1200	0.26	25.6
60	34	0.85	1200	0.23	24.2
61	36	0.90	1200	0.21	23.1
62	38	0.95	1200	0.21	24.3
63	20	0.50	1400	0.35	55.4
64	25	0.62	1400	0.34	47.9
65	30	0.75	1400	0.33	43.9
66	32	0.80	1400	0.29	33.0
67	34	0.85	1400	0.26	27.8
68	10	0.25	1400	0.37	71.9
69	15	0.37	1400	0.37	64.1
70	20	0.50	1400	0.35	56.2
71	25	0.62	1400	0.28	42.4
72	30	0.75	1400	0.24	32.1
73	32	0.80	1400	0.22	26.7
74	34	0.85	1400	0.21	26.6
75	36	0.90	1400	0.17	23.6
76	25	0.62	1600	0.31	50.9
77	30	0.75	1600	0.29	45.9
78	32	0.80	1600	0.24	31.8
79	34	0.85	1600	0.24	27.7
80	10	0.25	1600	0.32	72.1
81	15	0.37	1600	0.32	64.1
82	20	0.50	1600	0.31	56.3
83	25	0.62	1600	0.24	42.8
84	30	0.75	1600	0.22	34.7
85	32	0.80	1600	0.21	29.4
86	34	0.85	1600	0.20	29.5
87	36	0.90	1600	0.19	29.2
88	38	0.95	1600	0.19	30.5
89	25	0.62	1800	0.29	53.6
90	30	0.75	1800	0.27	48.5
91	32	0.80	1800	0.27	40.1
92	34	0.85	1800	0.20	29.2
93	36	0.90	1800	0.17	27.4
94	15	0.37	1800	0.31	70.8
95	20	0.50	1800	0.32	65.5

(*continued on next page*)

Appendix A (*continued*)

Serial no.	P (bar)	P_R	G (kg/m^2 s)	Dryout quality	Heat flux (kW/m^2)
96	25	0.62	1800	0.22	45.7
97	30	0.75	1800	0.19	34.4
98	32	0.80	1800	0.20	32.2
99	34	0.85	1800	0.20	32.5
100	36	0.90	1800	0.16	29.5
101	38	0.95	1800	0.15	31.3
102	25	0.62	2000	0.23	49.1
103	30	0.75	2000	0.22	46.7
104	32	0.80	2000	0.23	39.6
105	34	0.85	2000	0.21	33.2
106	20	0.50	2000	0.32	73.1
107	25	0.62	2000	0.28	59.8
108	30	0.75	2000	0.18	37.6
109	32	0.80	2000	0.18	32.9
110	34	0.85	2000	0.15	30.4
111	36	0.90	2000	0.13	29.9

References

[1] J.G. Collier, Convective Boiling and Condensation, second ed., McGraw-Hill, New York, 1981, pp. 248–274.

[2] L.S. Tong, Boiling crisis and critical heat flux, Int. J. Heat Mass Transfer 16 (1973) 1659–1660.

[3] G.F. Hewitt, Critical heat flux in flow boiling, in: Sixth International Heat Transfer Conferences, Tronto, vol. 6, 1978, pp. 143–171.

[4] Y. Katto, Critical heat flux, Int. J. Multiphase Flow 20 (Suppl.) (1994) 1–51.

[5] Y. Katto, H. Ohno, An improved version of the generalized correlation of critical heat flux for the forced convective boiling in uniformly heated vertical tubes, Int. J. Heat Mass Transfer 27 (1984) 1641–1648.

[6] P.B. Whalley, P. Hutchinson, G.F. Hewitt, The calculation of critical heat flux in forced convective boiling, in: Fifth International Heat Transfer conference, Tokyo, Paper No. B6.11, 1974.

[7] G.F. Hewitt, A.H. Govan, Phenomenological modelling of non-equilibrium flows with phase change, Int. J. Heat and Mass Transfer 33 (1990) 229–242.

[8] U.S.S.R Academy of Sciences, Tabular data for calculating burnout when boiling water in uniformly heated round tubes, Therm. Engng., Sept., 77–79; Teploenergitika, 23 (1976) 90–92.

[9] D.C. Groeneveld, Prediction of critical heat flux (CHF) for non-aqueous fluids in forced convective boiling, in: Proceeding of the 8th International Heat Transfer Conference, San Francisco, USA, vol. 5, 1986.

[10] D.C. Groeneveld, L.K.H. Leung, F.J. Erbacher, P.L. Kirillov, V.P. Bobkov, W. Zeggel, An improved look-up table method for predicting critical heat flux, in: Proceedings NURETH-6, Sixth International Topical Meeting on Nuclear Reactor Thermal Hydraulics, vol. 1, 1993, pp. 223–230.

[11] D.C. Groeneveld, S.C. Cheng, T. Doan, The CHF look-up table a simple and accurate method for predicting critical heat flux, Heat Transfer Eng. 7 (1986) 46–62.

[12] D.C. Groeneveld, L.K.H. Leung, P.L. Kirillov, V.P. Bobkov, I.P. Smogalev, V.N. Vinogradov, X.C. Huang, E. Royer, The 1995 look-up table for critical heat flux in tubes, Nucl. Eng. Design 163 (1996) 1–23.

[13] N. Hoyer, Calculation of dryout and post-dryout heat transfer for tube geometry, Int. J. Multiphase Flow 24 (1998) 319–334.

[14] S. Jayanti, M. Valette, Prediction of dryout and post-dryout heat transfer at high pressures using a one-dimensional three-fluid model, Int. J. Heat Mass Transfer 47 (2004) 4895–4910.

[15] J.R. Thom, Two-phase heat transfer to new refrigerants, in: Proceedings of Tenth International Heat Transfer Conferences, Brighton, UK, SK-2, 1994, pp. 19–41.

[16] I.L. Pioro, D.C. Groeneveld, S.C. Cheng, S. Doerffer, A. Vasić, Yu.V. Antoshko, Comparison of CHF measurements in R-134a cooled tubes and the water CHF look-up table, Int. J. Heat Mass Transfer 44 (2001) 73–88.

[17] A.W. Bennett, G.F. Hewitt, H.A. Kearsey, R.K.F. Keeys, Measurement of burnout heat flux in uniformly heated round tubes at 1000 psia, UKAEA Rep. No. AERE-R5055, 1965.

[18] K.M. Becker, C.H. Ling, S. Hedberg, G. Strand, An experimental investigation of post dryout heat transfer, Department of Nuclear Reactor Engineering, Royal Institute of Technology report KTH-NEL-33, Stockholm, Sweden, 1983.

[19] S.Y. Ahmad, Fluid to fluid modeling of critical heat flux: A compensated distortion model, Int. J. Heat Mass Transfer 16 (1973) 641–662.

[20] D.C. Groeneveld, A general CHF prediction method for water suitable for reactor accident analysis, CENG Report DRE/ STT/SETRE/82-2-E/DG, 1982.

[21] M.M. Shah, Improved general correlation for critical heat flux during upflow in uniformly heated vertical tubes, Int. J. Heat and Fluid Flow 8 (1987) 326–335.